Advances in Concrete Construction, *Vol. 4, No. 1 (2016) 001-014*
DOI: http://dx.doi.org/10.12989/acc.2016.4.1.001

Spalling of heated high performance concrete due to thermal and hygric gradients

Binsheng Zhang*, Martin Cullen[a] and Tony Kilpatrick[b]

School of Engineering and Built Environment, Glasgow Caledonian University, Cowcaddens Road, Glasgow G4 0BA, Scotland, UK

(Received July 9, 2015, Revised March 20, 2016, Accepted March 24, 2016)

Abstract. In this study, high performance concrete beams and prisms with high content of PFA were heated to various temperatures up to 450 ºC at heating rates of 1 ºC/min, 3 ºC/min and 10ºC/min. The thermal gradient was found to increase first with the heating time until a peak value was reached and then decrease until the thermal equilibrium was reached, measured as 115 ºC, 240 ºC and 268 ºC for the three heating rates. Spalling occurred on some specimens when the heating temperature was over 400 ºC for heating rates of 3 ºC/min and 10 ºC/min. The hygric gradient was found to reach its maximum when the thermal gradient reached its peak. This study indicates that spalling of HPC could happen when the heating temperature was high enough, and both thermal and hygric gradients reached their maxima.

Keywords: high performance concrete; spalling; high temperature; thermal gradient; hygric gradient

1. Introduction

Nowadays, high strength and ultra-high strength concrete has been largely used for modern constructions, e.g. tall reinforced concrete buildings, long prestressed concrete bridges, cooling towers in power plants, prestressed concrete pressure vessels in nuclear power stations, tunnels, etc. When the high performance concrete with high strength, high toughness and low porosity exposed to rapidly elevated temperatures, it sustains severe physical and chemical changes. Physical effects include large volume changes due to thermal dilations, thermal shrinkage and creep associated with water loss. The volume changes can result in large internal stresses and lead to micro cracking and fractures. Depending on heating rates and hygroscopic boundary conditions, the rapid exposure to high temperatures with high pressures can lead to explosive spalling of concrete and potentially disastrous accidents. High temperatures also cause chemical and micro-structural changes, such as migration of water (diffusion, drying), increased dehydration, interfacial thermal incompatibility and chemical decomposition of hardened cement paste and aggregates. In general, exposure to high temperatures, the mechanical and structural characteristics of high performance concrete including strength, stiffness and toughness will be largely degraded

*Corresponding author, Ph.D., E-mail: Ben.Zhang@gcu.ac.uk
[a]Ph.D., E-mail: M.N.Cullen@gcu.ac.uk
[b]MSc, E-mail: A.R.Kilpatrick@gcu.ac.uk

http://www.techno-press.org/?journal=acc&subpage=7 ISSN: 2234-0912 (Print), 2234-179X (Online)

(Zhang *et al*. 2000, 2002b, Zhang and Bićanić 2002a, 2006, Zhang 2011).

Much research has been conducted on various aspects on spalling of high performance concrete, in particular caused by fire, including mechanisms (Castillo and Durrani 1990, Morita *et al.* 1999, Sullivan 2001, Ali 2002, Arita *et al.* 2002, Hertz 2003, Kodur and Phan 2007, Zhang 2011, Kanéma *et al.* 2011, Ko *et al.* 2011), testing methods (Hertz and Sørensen 2005), numerical modelling (Ozbolt *et al.* 2005, Dwaikat and Kodur 2008, 2009a, Zeimal *et al.* 2008, Zhao *et al.* 2011, Zhang and Davie 2013), fire resistance of structural members (Kodur 1998, Ali *et al.* 2001, Savov *et al.* 2005, Dwaikat and Kodur 2009b, Zheng *et al.* 2010), protection (Bentz 2000, Kodur 2000), etc. Hertz (2003) and Kodur and Phan (2007) systematically summarised the critical factors governing the fire performance and possible spalling of high strength concrete, including fire characteristics (fire type, fire size and heat output), material characteristics (concrete strength, water-cement ratio, silica fume, concrete moisture content, concrete density, fibre type and content, reinforcement, aggregate type and age of concrete exposed to fire) and structural features (specimen size, lateral reinforcement, restraint degree, and load intensity and type). In general, the factors largely contributing to spalling of high performance concrete are considered to be low concrete porosity and permeability, large thermal gradient and stresses, and large hygric gradient and fast moisture migration. High thermal and hygric gradients are solely caused by high heating temperatures and high heating rate.

In this study, the effects of heating scenarios on behaviour and possible spalling of the high performance concrete was investigated on beam and prism specimens heated to varied temperatures up to 450ºC at different heating rates. The thermal gradients, the differences between the environmental temperature in the furnace and the temperature at the centre of the concrete specimens were continuously monitored. Meanwhile, the weight losses of the concrete specimens during heating and exposure stages representing the moisture evaporation and hygric gradients were also continuously measured. Thus, the crucial factors contributing to spalling of high performance concrete could be assessed accordingly.

2. Experimental

2.1 Concrete specimens

For the complete test series, eight heating temperatures were adopted as T_m = 105 ºC, 150 ºC, 200 ºC, 250 ºC, 300 ºC, 350 ºC, 400 ºC and 450 ºC, respectively, together with three heating rates $\dot{T}^+ = (dT/dt)^+$ = 1 ºC/min, 3 ºC/min and 10 ºC/min. The exposure time at a designated temperature was fixed at t_h = 4 hours, 8 hours and 16 hours, respectively. Cooling was conducted by leaving the furnace either fully closed or fully open to obtain slow and fast cooling conditions. A total of 240 beams were tested with at least three beams for each scenario, and 140 prisms were tested only for residual Young's modulus. As bench marks, five beams and three prisms were tested at 20 ºC.

The primary fracture parameters measured under both hot and cold conditions were the fracture energy G_F, fracture toughness K_{IC} and the modulus of rupture f_r. The residual material properties measured were the compressive strength f_{cu}, splitting tensile strength f_t', Young's modulus E and concrete density ρ. The weight loss ω was continuously measured when the concrete was heated and could be used to further study its effect on the fracture behaviour of concrete during heating. Part of the test data for the above mentioned parameters for different heating scenarios have been

Table 1 Concrete mix design in weight

Contents	OPC	PFA	Quartz sand	10 mm dolerite	20 mm dolerite	Water	Plasticizer
Weight ratio	1	0.33	2.45	1.39	2.78	0.56	0.006
Quantities (kg/m^3)	300	99	735	417	834	168	1.8

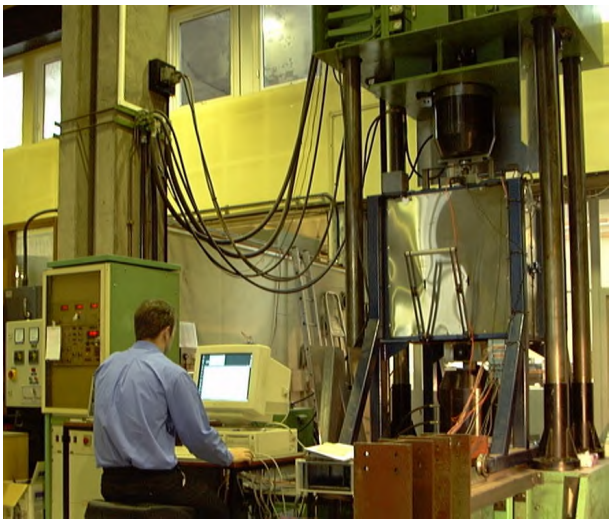

Fig. 1 A programme-controlled furnace with the 2000 kN LOS testing machine

reported in the previous publications (Zhang and Bićanić 2006, Zhang 2011, Zhang *et al*. 2013).

Notched concrete beams of 500 mm×100 mm×100 mm, with a 400 mm effective span and a 50 mm notch depth, were loaded under three-point bending for determining G_F, K_{IC} and f_r. Notches were prepared using a diamond saw before being heated. Concrete prisms of 200 mm×100 mm× 100 mm were cast for determining the residual E, three for each scenario. To effectively utilise the heated concrete, 100 mm cubes were cut from the broken beams for obtaining f_{cu} and f_t'.

The 42.5N OPC and Pulverised Fuel Ash were adopted as adhesive materials. The aggregates included the calcareous quartz sand, the 10 mm single-sized and 20 mm graded quartz dolerite (basalt type). Pozzolith 300 N plasticiser was used for achieving a slump of 125 mm. The concrete mix design is listed in Table 1. The test age was at least 90 days to allow full hydration, giving f_{cu} = 67.1 MPa, f_t' = 4.47 MPa, E = 35.6 GPa and ρ = 2463 kg/m^3.

2.2 Heating furnace and temperature measurements

A program-controlled three-zone VTS furnace (600 ± 5 ºC) was specially designed and it had two identical halves with an inner dimension of 800 mm×600 mm×600 mm. There were three independent heating zones from top to bottom, which helped the concrete to be heated uniformly and efficiently. Each zone consisted of six 1.5 kW Ni-chrome heating elements so the furnace had a total of 18 heating elements with a power of 27 kW. Each zone had its own thermocouple to control the temperature. The bottom zone was the master zone for the overall control with the middle and top zones as the slave ones. In the top zone, an extra thermocouple was used to prevent

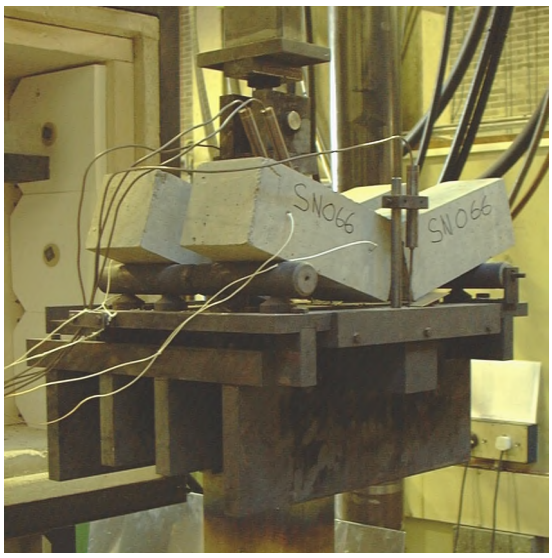

Fig. 2 N-type thermocouples embedded in the beam specimens

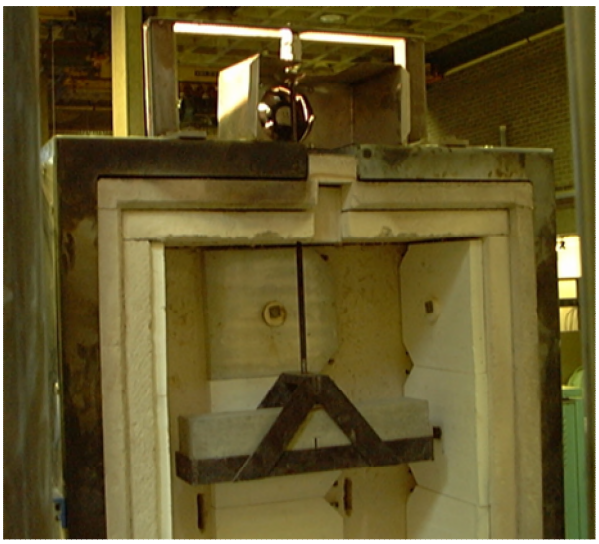

Fig. 3 Load cell linked to the steel cradle with the beam specimen

the furnace from overheating. If the temperature in the top zone was higher than the pre-set limit, the power for the furnace would be automatically switched off. Fans were used to circulate the air in the furnace for heating the concrete uniformly and cooling the loading pieces. The furnace was built around a 2000 kN LOS universal testing machine to allow the tests to be conducted at high temperatures. Fig. 1 shows the furnace with the testing machine and the control panel.

To continuously monitor the temperatures inside the concrete beams, N-type thermocouples were embedded in the beams which were used for three-point bending tests. Two positions were chosen for each beam: 50 mm close to the edge (side hole) and 50 mm away from the centre (middle hole) to avoid disturbing the notched mid-section, see Fig. 2. The 50 mm deep holes were

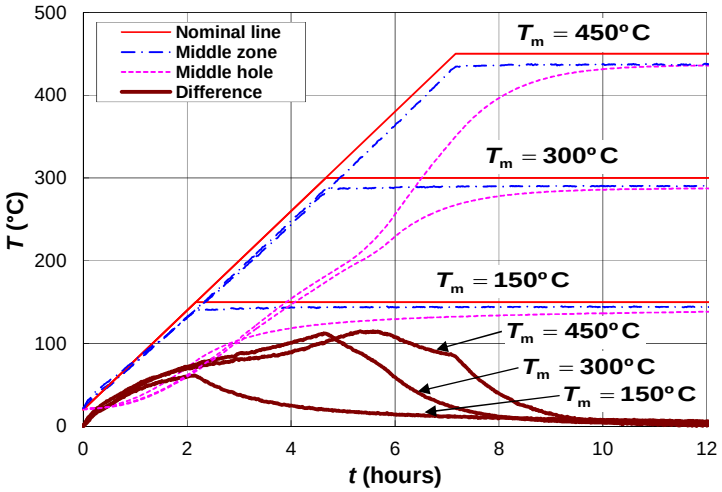

Fig. 4 Temperature developments in the furnace and concrete beams for 1ºC/min

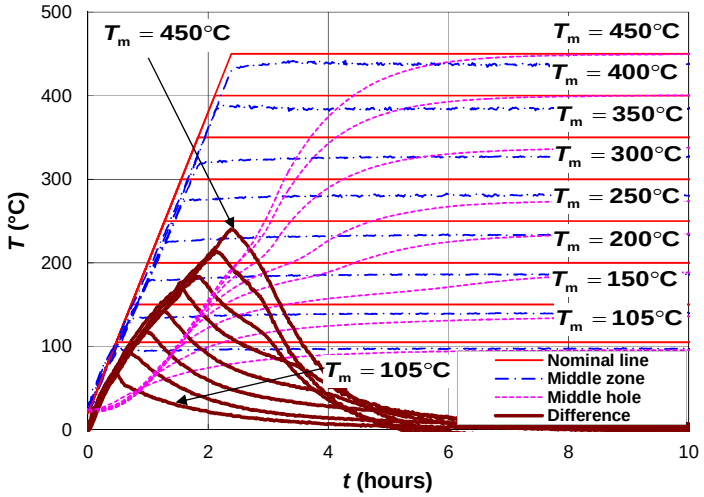

Fig. 5 Temperature developments in the furnace and concrete beams for 3ºC/min

drilled before the beams were heated. The temperatures from the thermocouples in the three heating zones and from the master thermocouple controlling the furnace were recorded.

2.3 Weight loss measurement

For continuously monitoring the moisture migration during heating, exposure, testing and cooling, two steel cradles were made for holding concrete beams, each connected to a VC8000 high precision load cell of 25 kg ± 10 g, fixed outside the furnace. During heating, exposure and cooling, the weight changes were recorded every 5 seconds. During testing, the weight changes were recorded together with the load and displacements every half a second. Fig. 3 shows a cradle

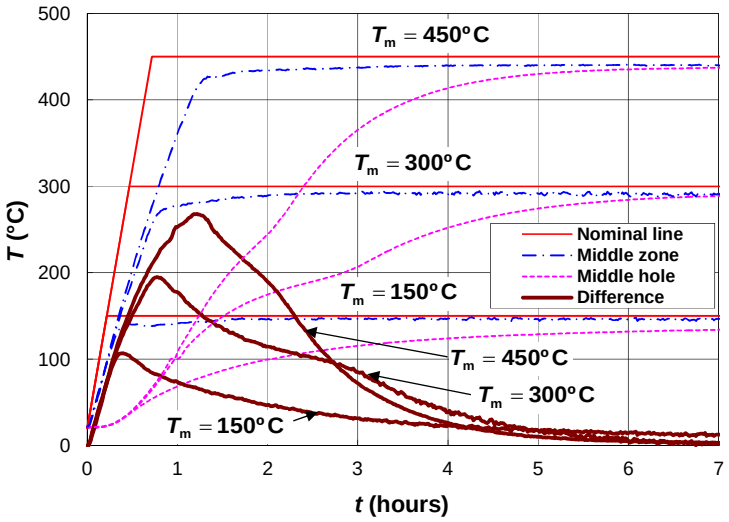

Fig. 6 Temperature developments in the furnace and concrete beams for 10ºC/min

with the concrete beam in the furnace, which was connected to the external load cell via a steel bar.

3. Temperauture developments, thermal gradients and spalling

3.1 Temperature developments in the furnace

Because previous research indicated that spalling could only happen during the heating stage, much attention was paid to this stage of heating history. Figs. 4-6 illustrate the temperature developments in the middle zone of the furnace for the heating rates $\dot{T}^+$ = 1 ºC/min, 3 ºC/min and 10 ºC/min, respectively. As reference, the nominal heating temperature versus time curves are also included in the figures. It can be seen that the difference between the temperature in the middle heating zone and the nominal temperature for three heating temperatures is very small for $\dot{T}^+$ = 1 ºC/min regardless of heating temperature target. The middle zone temperature reasonably matched the nominal one for $\dot{T}^+$ = 3 ºC/min. For $\dot{T}^+$ = 10 ºC/min, however, the middle zone temperature did not match the nominal one at all during the heating process and typically reached the nominal one with a delay for about two hours.

3.2 Temperature developments in the concrete

Two thermocouples were embedded in the concrete to monitor the temperature developments near the edge (edge hole) and the centre of the furnace (middle hole). Because the temperature within the furnace was found to be reasonably uniform due to good circulation, the lowest temperature within the concrete should come from the thermocouples in the middle hole and was used for analysis. The temperature developments inside the concrete from the thermocouples in the

Table 2 Peaks for thermal gradients and the corresponding heating temperatures

$\dot{T}^+$ (ºC/min)	1	3	10
T_{max} (°C)	ΔT_{max} (°C)	ΔT_{max} (°C)	ΔT_{max} (°C)
105	/	69.6	/
150	64.4	99.1	107.2
200	/	122.5	/
250	/	147.6	/
300	112.9	169.9	197.8
350	/	190.1	/
400	/	209.9	/
450	120.8	229.3	258.5

middle holes for the heating rates $\dot{T}^+$ = 1ºC/min, 3 ºC/min and 10 ºC/min are also included in Figs. 4-6.

During the heating process, the temperature curves follow the order from high to low: nominal, middle zone and middle hole. The temperature development in the middle hole was always far behind that of the middle zone. For each heating rate, each temperature developed followed the same path regardless of the heating temperature targets during the heating process. With the increasing heating time, these curves become closer, which means that the temperature inside the concrete beams tended to become more uniform, i.e. the temperature inside the concrete would gradually approach the surrounding heating temperature and eventually become fully uniform over the whole concrete. In other words, the thermal equilibrium would be reached for all concrete specimens in the furnace. It took 12 hours to reach such a thermal equilibrium state for $\dot{T}^+$ = 1 ºC/min, 8 hours for $\dot{T}^+$ = 3 ºC/min and only 6 hours for $\dot{T}^+$ = 10ºC/min.

3.3 Temperature differences in the concrete and thermal gradients

The heating rate plays a dominant role in determining the behaviour of concrete. After a thermal equilibrium state is reached, the absolute heating temperature level will greatly influence the behaviour of concrete together with the exposure time. The effects of heating or cooling rates on the concrete behaviour can be related using the thermal gradient within the concrete. If the difference is very small or the thermal gradient is fairly equal to zero, a thermal equilibrium state is reached and the heating rate may no longer influence the behaviour of concrete. Figs. 4-6 also include the differences between the temperature in the middle heating zone and the one in the middle hole of the heated concrete beams for the heating rates $\dot{T}^+$ = 1ºC/min, 3ºC/min and 10ºC/min, respectively. This temperature difference actually represents the maximum thermal gradient within the concrete specimens.

During the heating process, the temperature difference generally increased from zero with the heating time until the maximum value was reached. Thereafter it decreased and eventually dropped to zero again. The final state was corresponding to the thermal equilibrium state. For $\dot{T}^+$ = 1 ºC/min and 3 ºC/min, the maximum values or the peaks of the temperature difference versus heating time curves happened in the heating stage. For $\dot{T}^+$ = 10 ºC/min, however, the peaks for the curves occurred in the exposure stage. The corresponding peak values and heating times were

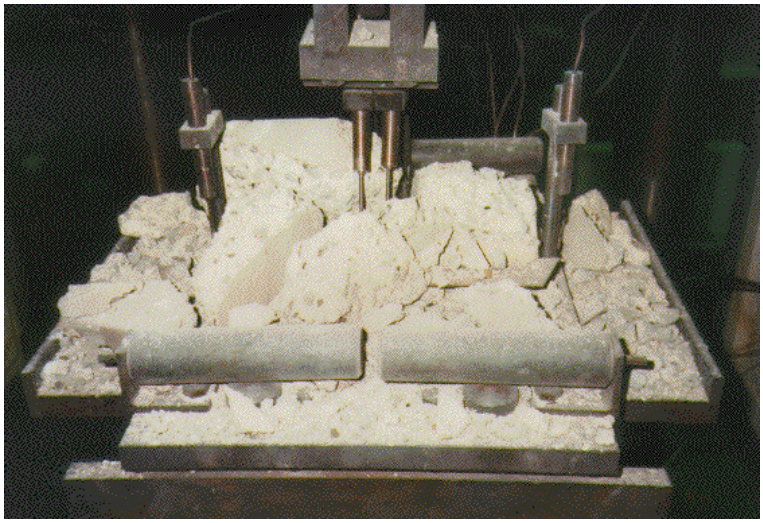

Fig. 7 Spalling of the concrete beams on the testing block for 3ºC/min

Fig. 8 Partial spalling of a concrete prism in the cradle for 10ºC/min

also largely dependent on the heating rate. Table 2 lists the average peak values of the temperature difference or the thermal gradients for various heating temperatures and heating rates. For $\dot{T}^+$ = 1 ºC/min, the peaks occurred just before the heating stage was finished for T_m = 150 ºC and 300 ºC but far before this stage was finished for T_m = 450 ºC. The corresponding peak values, ΔT_{max}, were 64.4 ºC, 112.9 ºC and 120.8 ºC, respectively, for these three heating temperatures. For $\dot{T}^+$ = 3 ºC/min, the peaks always occurred while the heating stage was almost finished for all heating temperatures from 105 ºC to 450 ºC. Typically, the peak values were ΔT_{max} = 99.1 ºC, 169.9 ºC and 229.3 ºC for T_m = 150 ºC, 300 ºC and 450 ºC, respectively. For $\dot{T}^+$ = 10ºC/min, three peaks occurred corresponding to a time which was about 70% longer than the heating time, with the peak values ΔT_{max} = 107.2 ºC, 197.8 ºC and 258.5 ºC for T_m = 150 ºC, 300 ºC and 450 ºC, respectively.

Table 3 Weight loss for different heating temperatures and heating rates

$\dot{T}^+$ (ºC/min)	1	3	10
T_{max} (°C)	ω_u (%)	ω_u (%)	ω_u (%)
105	/	2.46	/
150	4.47	4.59	4.64
200	/	5.16	/
250	/	5.58	/
300	5.87	5.97	6.09
350	/	6.28	/
400	/	6.62	/
450	6.65	6.76	6.85

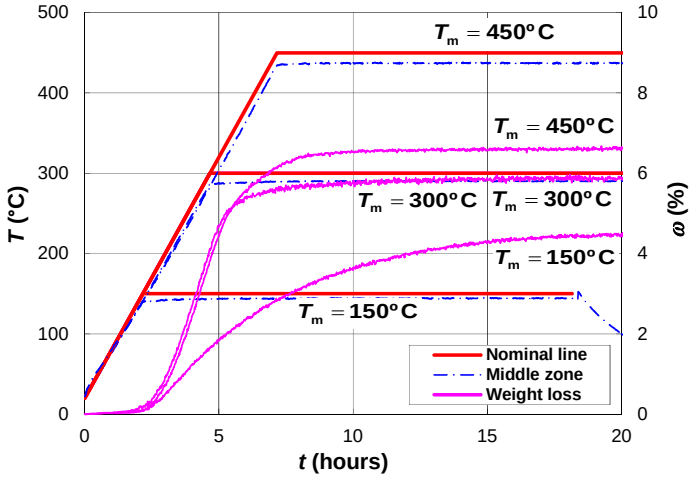

Fig. 9 Weight loss in the complete heating-exposure-cooling process for 1 ºC/min

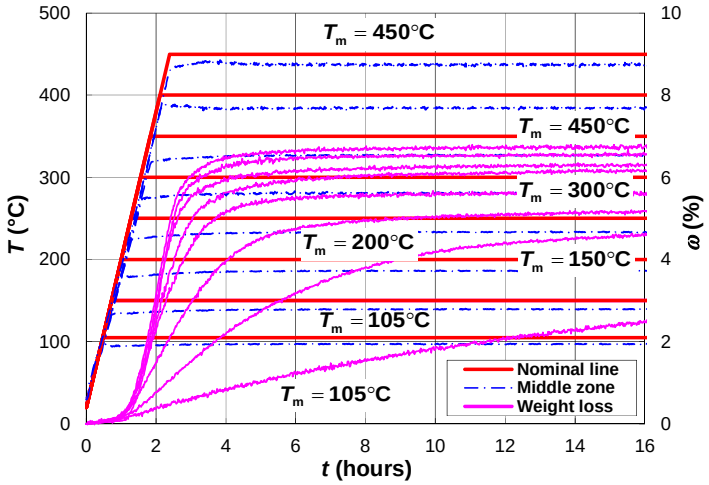

Fig. 10 Weight loss in the complete heating-exposure-cooling process for 3 ºC/min

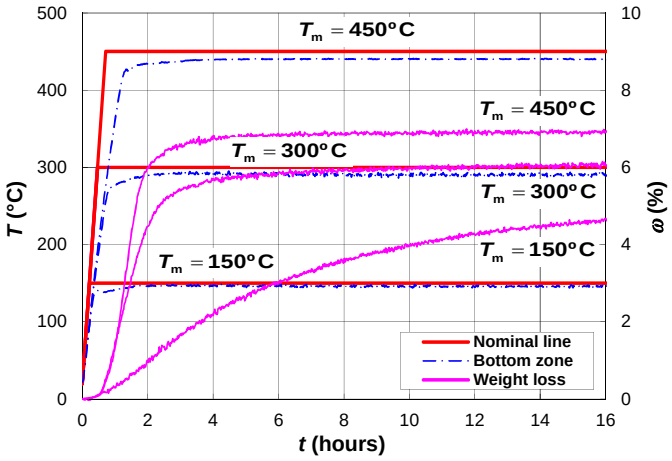

Fig. 11 Weight loss in the complete heating-exposure-cooling process for 10ºC/min

3.4 Spalling of the concrete

In this study, seven out of 28 concrete beam specimens subjected to a heating temperature T_m = 450 ºC for $\dot{T}^+$ = 3 ºC/min failed due to heavily explosive spalling, and the rest twenty-one beams survived from spalling. The moment for the spalling was exactly corresponding to the peak point of the thermal gradient versus heating time curve with the heating temperature T varying between 400 ºC and 430 ºC. No spalling happened for the heating temperatures below 400 ºC. For $\dot{T}^+$ = 10ºC/min, several prisms failed due to spalling, but no spalling happened to the concrete beams at this rate perhaps due to a small number of beams (a total of seven) that were heated. Fig. 7 shows the spalling failure of two concrete beams on the loading block for $\dot{T}^+$ = 3 ºC/min, and Fig. 8 shows the spalling failure of a concrete prism in the cradle for $\dot{T}^+$ = 10 ºC/min. There was no spalling failure at all for any beam and prism specimens for the heating rate of 1 ºC/min. In the preliminary work done by the authors (Zhang *et al.* 2000), no spalling failure happened for all the heated normal and high strength concrete beams because they were more porous.

4. Weight loss and hygric gradients

4.1 Weight loss during the complete heating, exposure and cooling process

In this study, two VC8000 25 kg high precision load cells were used to continuously monitor the weight loss during the heating, exposure and cooling process. Readings were taken as often as possible to make statistical study possible and to eliminate the errors caused by the load cells. Here, the time interval for the date taking was adopted as five seconds. Thereafter, every twelve sets of data were averaged again using a FORTRAN program to represent the results for every minute. Figs. 9-11 illustrate the continuous developments of the averaged weight loss for the fixed exposure time of 16 hours but different heating rates ($\dot{T}^+$ = 1 ºC/min, 3 ºC/min and 10 ºC/min). No data for the fast cooling were available because the load cells were severely damaged by the

spalling before these tests took place. The weight loss at any time can be found from these figures. The middle zone temperature is chosen here to represent the environmental heating temperature, with the nominal lines plotted in these figures as the references.

4.2 Hygric gradients during the heating and exposure stages

The results show that the weight loss ω is a monotonically increasing function of heating time. The weight loss process with heating time can generally be divided into three stages. The slopes of the weight loss versus heating time curves actually represent the hygric gradients within the concrete.

In the first stage, ω increased very little with the heating time at a small increase rate. The ω - t curves are concave, and this stage only lasted a few hours. The actual length of the period was largely dependent on the heating rate but almost independent from the heating temperature level. For a given heating rate, the weight loss followed the same pattern. With the increase of the heating rate, this time length became shorter. For $\dot{T}^+$ = 1 ºC/min, it was about 3 hours. However, it became shortened to less than 2 hours for $\dot{T}^+$ = 3 ºC/min and only 1 hour for $\dot{T}^+$ = 10 ºC/min. In other words, the hygric gradient in the concrete gradually increased in this stage, which was caused by the corresponding increasing thermal gradient.

In the second stage, ω increased rapidly with the heating time. The corresponding increase rate or the hygric gradient gradually surged and then gradually decreased after a maximum was reached. The corresponding ω - t curves becoming convex. During this stage, the weight loss increased from very little to large values. The actual time length for this stage was dependent not only on the heating rate but also on the heating temperature level. It decreased with both the increasing heating rate and the increasing heating temperature level. For $\dot{T}^+$ = 1 ºC/min, this stage lasted about 20 hours for T_m = 150 ºC, and 5 hours for T_m = 300 ºC and 450 ºC. For $\dot{T}^+$ = 3 ºC/min, this stage lasted 16 hours for T_m = 150 ºC, and 3 hours for T_m = 300 ºC and 450 ºC. For $\dot{T}^+$ = 10 ºC/min, it lasted 15 hours for T_m = 150ºC, but less than 3 hours for T_m = 300 ºC and 450 ºC. There was no big difference in the time length for the heating temperature level above 300 ºC or the heating rate over 3ºC/min.

In the third and final stage, ω slightly increased with the heating time at a decreased rate and eventually reached a stable value. In other words, the hygric gradient only slightly increased and a hygric equilibrium state was reached for which the ultimate weight loss would no longer increase. Except for the case of the heating temperature below 150ºC, the weight loss became stable for all other heating temperatures. If the exposure time was long enough, the heating temperature level would become the only factor to influence the ultimate steady state values of the weight loss.

Table 3 lists the values of the final steady state weight loss after the 16-hour exposure time and a slow cooling for different heating temperatures and three heating rates. For each heating temperature, a higher heating rate just caused a slightly higher weight loss but this change was almost negligible. For T_m = 150 ºC, the values of the weight loss ω_u were 4.47%, 4.59% and 4.64% for $\dot{T}^+$ = 1 ºC/min, 3 ºC/min and 10 ºC/min, respectively. For T_m = 300 ºC, the corresponding values of ω_u were 5.87%, 5.97% and 6.09%. Finally for T_m = 450 ºC, the corresponding values of ω_u were 6.65%, 6.76% and 6.85%, respectively.

5. Brief discussion

There are at least three conditions under which spalling may occur. The first condition is that

the heating temperature must be high enough. From this study, the heating temperature must be over 400 ºC. The second one is that the heating rate must be high enough so as to produce a high thermal gradient and a high hygric gradient. In this study, the heating rate was 3 ºC/min or over for such case. The third condition is the concrete must be very dense with lower porosity and smaller pore sizes. In this study, a big content of PFA was used and very fine particles filled the big pores and blocked the access for moisture to migrate from the very depth of the concrete.

6. Conclusions

In this study, the high performance concrete beams and prisms with high content of PFA were heated to various temperatures up to 450 °C with heating rates of 1 °C/min, 3 °C/min and 10 °C/min. The explosive spalling was observed.

The spalling only happened for those concrete specimens heated toward 450°C with the heating rates of 3 °C/min and 10 °C/min, but did not happen for the heating rate of 1 °C/min or lower heating temperatures.

The temperature developments in the furnace environment and inside the concrete were continuously monitored. Spalling only happened when the difference between the environmental temperature in the furnace and the temperature inside the concrete, or the thermal gradient, reached its maximum. No further spalling would happen if the concrete passed over this critical thermal gradient peak.

The weight loss of the concrete was also continuously monitored. Spalling happened when the slope of the weight loss versus heating time curve, or the hygric gradient reached its maximum.

Acknowledgments

This project was conducted under the British Energy contract PP/120543/DGD/HN.

References

Ali, F.A. (2002), “Is high performance concrete more susceptible to explosive spalling than normal strength concrete in fire?”, *Fire Mater.*, **26**(3), 127-130.

Ali, F.A., O’Connor, D. and Abu-Tair, A. (2001), “Explosive spalling of high-strength concrete columns in fire”, *Mag. Concrete Res.*, **53**(3), 197-204.

Arita, F., Harada, K. and Miyamoto, K. (2002), “Thermal spalling of high-performance concrete during fire”, *Second International Workshop on Structures in Fire*, Christchurch, New Zealand, 253-261.

Bentz, D. (2000), “Fibers, percolation, and spalling of high-performance concrete”, *ACI Mater. J.*, **97**(3), 351-359.

Castillo, C. and Durrani, A.J. (1990), “Effect of transient high temperature on high-strength-concrete”, *ACI Mater. J.*, **87**(1), 47-53.

Dong, X., Ding, Y. and Wang, T. (2008), “Spalling and mechanical properties of fiber reinforced high-performance concrete subjected to fire”, *J. Wuhan University of Tech. - Mater. Sci. Ed.*, 743-749.

Dwaikat, M.B. and Kodur, V.K.R. (2008), “A numerical approach for modeling the fire induced restraint effects in reinforced concrete beams”, *Fire Safety J.*, **43**(4), 291-307.

Dwaikat, M.B. and Kodur, V.K.R. (2009a), “Hydrothermal model for predicting fire-induced spalling in concrete structural systems”, *Fire Safety J.*, **44**(3), 425-434.

Dwaikat, M.B. and Kodur, V.K.R. (2009b), “Fire induced spalling in high strength concrete beams”, *Fire Tech.*, **46**(1), 251-274.

Hertz, K.D. (2003), "Limits for spalling of fire-exposure concrete", *Fire Safety J.*, **38**(2), 103-116.
Hertz, K.D. and Sørensen, L.S. (2005), "Test method for spalling of fire exposure concrete", *Fire Safety J.*, **40**(5), 466-476.
Kanéma, M., Pliya, P., Noumowé, A. and Gallias, J. (2011), "Spalling, thermal, and hydrous behavior of ordinary and high-strength concrete subjected to elevated temperature", *J. Mater. Civil Eng.*, **23**(7), 921-930.
Ko, J., Ryu, D. and Noguchi, T. (2011), "The spalling mechanism of high strength concrete under fire", *Mag. Concrete Res.*, **63**(5), 357-370.
Kodur, V.K.R. (1998), "Fire performance of high-strength concrete structural members", *Can. J. Civil Eng.*, **25**(6), 975-981.
Kodur, V.K.R. (2000), "Spalling in high-strength concrete exposed to fire: concerns, causes, critical parameters and cures", *Adv. Tech. Struct. Eng.*, Ed by Mohamed Elgaaly P.E., 1-9.
Kodur, V.K.R. and Phan, L. (2007), "Critical factors governing the fire performance of high strength concrete systems", *Fire Safety J.*, **42**(6), 482-488.
Morita, T., Nishida, A. and Yamazaki, N. (1999), "An experimental study on spalling of high strength concrete elements under fire attack", *Fire Safety Science - the Proceeding of the Sixth International Symposium*, July 5-9, 1999, Poitiers, France, 855-866.
Ozbolt, J., Kozar, I., Eligehausen, R. and Periskic, G. (2005), "Three-dimensional FE analysis of headed stud anchors exposed to fire", *Comput. Concrete*, **2**(4), 249-266.
Savov, K., Lackner, R. and Mang, H.A. (2005), "Stability assessment of shallow tunnels subjected to fire load", *Fire Safety J.*, **40**(8), 745-763.
Sullivan, P.J.E. (2001), "Deterioration and spalling of high strength concrete under fire", *Offshore Technology Report 2001/074*, City University, London.
Zeimla, M., Lacknera, R., Pesaventoc, F. and Schrefler, B.A. (2008), "Thermo-hydro-chemical couplings considered in safety assessment of shallow tunnels subjected to fire load", *Fire Safety J.*, **43**(2), 83-95.
Zhang, B. (2011), "Effects of moisture evaporation (weight loss) on fracture properties of high performance concrete subjected to high temperatures", *Fire Safety J.*, **46**(8), 543-549.
Zhang, B. and Bićanić, N. (2002a), "Residual fracture toughness of normal- and high-strength gravel concrete after heating to 600 °C", *ACI Mater. J.*, **99**(3), 217-226.
Zhang, B. and Bićanić, N. (2006), "Fracture energy of high-performance concrete at high temperatures up to 450°C: the effects of heating temperatures and testing conditions (hot and cold)", *Mag. Concrete Res.*, **58**(5), 277-288.
Zhang, B., Bićanić, N., Pearce, C.J. and Balabanic, G. (2000), "Residual fracture properties of normal- and high-strength concrete subject to elevated temperatures", *Mag. Concrete Res.*, **52**(2), 123-136.
Zhang, B., Bićanić, N., Pearce, C.J. and Phillips, D.V. (2002b), "Relationship between brittleness and moisture loss of concrete exposed to high temperatures", *Cement Concrete Res.*, **32**(3), 363-371.
Zhang, B., Cullen, M. and Kilpatrick, T. (2013), "Fracture toughness of high performance concrete subjected to elevated temperatures: the effects of heating temperatures and testing conditions (hot and cold)", *The 2013 International Conference on Computational Technologies in Concrete Structures*, 8-12 September 2013, Jeju, Korea.
Zhang, H.L. and Davie, C.T. (2013), "A numerical investigation of influence of pore pressures and thermally induced stresses for spalling of concrete exposed to elevated temperatures", *Fire Safety J.*, **59**, 102-110.
Zhao, J., Zheng, J.J., and Peng, G.F. (2011), "Fire spalling modeling of high performance concrete", *Appl. Mech. Mater.*, **52-54**, 378-383.
Zheng, W.Z., Hou, X.M., Shi, D.S. and Xu, M.X. (2010), "Experimental study on concrete spalling in prestressed slabs subjected to fire", *Fire Safety J.*, **45**(5), 283-297.